A variational approach for calculating Auger electron spectra: going beyond the impurity approximation

Anamitra Mukherjee,[1] George A. Sawatzky,[1,2,3] and Mona Berciu[1,2]

[1] *Department of Physics and Astronomy, University of British Columbia, Vancouver, BC, Canada, V6T 1Z1*
[2] *Quantum Matter Institute, University of British Columbia, Vancouver, BC, Canada, V6T 1Z4*
[3] *Department of Chemistry, University of British Columbia, Vancouver, BC, Canada, V6T 1Z1*

(Dated: January 21, 2013)

We propose a novel variational method to calculate the two-hole propagators relevant for Auger spectroscopy, which can be thought of as an intermediary step between the full solution (which is difficult to generalize to systems with partially filled bands) and the impurity approximation. Like the former, our solution has the full translational invariance, and like the latter, it can be generalized to systems with partially filled bands. Here, we compare both our variational approximation and the impurity approximation against the exact solution for a simple one-dimensional model with filled bands, and show that when both are valid, the variational approximation is superior.

I. INTRODUCTION

Spectroscopic measurements are a powerful set of tools for probing various aspects of many-body physics.[1,2] Among these, Auger electron spectroscopy (AES) provides information about the local atomic multiplet structure, on-site interaction strengths and the crystal fields.[3–5] In transition metal oxides, the AES of the transition element can be supplemented by the O *KLL* Auger spectra, resulting in additional information about the O on-site repulsion energy as well as interactions between holes located on nearest-neighbor transition metal and O ions.[6] Such information is vital for understanding correlated materials, which is why AES has been the subject of sustained research for a long time.

The Auger process consists of the decay of a core hole into two final state holes plus an Auger electron, and is mediated by onsite Coulomb interactions. The two final state holes are initially located on the atomic site where the original core hole was created by the high energy X-ray. One of the most studied cases has these two final state holes residing in the valence band, and goes by the name of Core-Valence-Valence (CVV) Auger spectroscopy. From a theoretical point of view, the easiest case to handle has a full valence band except for the two Auger holes. The central quantity of interest is the two hole Green's function, which for an otherwise full band can be calculated within the two-step approximation using the Cini-Sawatzky theory.[7–9] The resulting two hole spectral function, multiplied by momentum dependent matrix element factors, provide the theoretical predictions for AES.[10] Many extensions of this approach have been carried out to incorporate various aspects such as dynamical screening,[11–13] off-site interactions,[14] overlap effects,[15–17] and one step formulation.[18] We refer the reader to a recent review[19] for more details. These efforts have led to spectacular success in explaining AES for materials such as Cu and Cu_2O.

However, the problem of understanding AES for systems with a partially filled valence band, for example the oxides of transition elements Ni, Co, Fe, Mn, etc., remains open, because the two hole spectral function is very challenging to compute in this case. Limited success has been achieved employing variants of the bare ladder approximations[20] and assuming low hole density in the bands. A completely different approach is to use the Anderson impurity approximation, whose underlying idea is as follows: in transition metal oxides, the transition metal atoms are typically connected to each other through oxygen ligands. The simplest example in one dimension is sketched in Fig. 1(a), and has transition metal atoms intercalated with O atoms. In the impurity approximation,[21–24] the full problem is simplified to that of a single transition metal atom coupled to the bath of O, as sketched in Fig. 1(b). This greatly simplifies the calculation and is a reasonable step towards understanding local multiplet structures. However, because the symmetry of the problem is lowered, momentum-resolved spectral weights cannot be calculated.

Here, we propose a variational approach for finding the two-hole Green's functions needed for AES, which can be thought of as an intermediary step between the impurity approximation and the full lattice calculation. Like the former, it has a reduced Hilbert space and can therefore be generalized quite easily to systems with partially filled bands. Like the latter, it has full translational invariance so that momentum-resolved spectral weights can be calculated. We argue that the location of the spectral weight components ignored within our approximation can be inferred apriorily but should be small for oxides and other

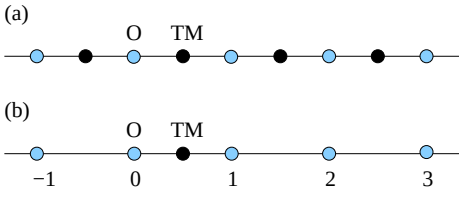

FIG. 1. (a) Sketch of the 1D periodic Anderson model. 'TM' and 'O' represent transition metal and O ions, respectively. (b) In the impurity approximation, an impurity 'TM' ion is coupled to the 1D 'bath' of O.

materials where AES is a useful probe. Moreover, the variational space can be systematically enlarged to verify the relevance of some of the neglected terms.

In this paper we present the underlying idea and the general formalism of this variational approach, which is based on a recently developed method to calculate many-particle Green's functions.[25–27] Here, we apply it to the simple model sketched in Fig. 1 and assume otherwise full bands, so that we can benchmark it against the exact solution available in this case. For completness, we also show impurity approximation results for this model. This allows us to gauge the advantages and disadvantages of both these approximations and to understand for what regions in the parameter space our variational approximation is valid. This information will guide us, in future work, to using it for appropriate systems where the transition elements have partially filled d orbitals.

The paper is organized as follows. In Sections II we define the Hamiltonians and in Section III we discuss the methods to calculate two-hole propagators exactly and with the two approximations. In Section IV we present the exact results and compare them with those predicted by our variational approximation as well as the impurity approximation for two different topologies of coupling between the impurity and the bath of O. Section V contains the summary and conclusions. Some of the details are presented in the two Appendixes.

II. HAMILTONIAN

A. The periodic Anderson model

The periodic 1D Anderson model shown in Fig. 1(a), is defined by the Hamiltonian:

$$\mathcal{H}_{\mathcal{P}} = \mathcal{H}_{\rm TM} + \mathcal{H}_{\rm O} + \mathcal{H}_{\rm hyb}$$

where $\mathcal{H}_{\rm TM}$ describes the chain of TM atoms, which for simplicity are assumed to have only two (spin-degenerate) states each, and is given by:

$$\mathcal{H}_{TM} = U\sum_i n_{d,i,\uparrow}n_{d,i,\downarrow} + \Delta\sum_{i,\sigma} n_{d,i,\sigma}.$$

The O "bath" is described by a 1D Hubbard model:

$$\mathcal{H}_{\rm O} = -t\sum_{i,\sigma}(c^\dagger_{i,\sigma}c_{i+1,\sigma} + h.c.) + U_O\sum_i n_{i,\uparrow}n_{i,\downarrow}$$

while the TM-O hybridization is described by

$$\mathcal{H}_{hyb} = -V\sum_{i,\sigma}\left[d^\dagger_{i,\sigma}\left(c_{i,\sigma} + c_{i-1,\sigma}\right) + h.c.\right].$$

Here, all creation operators are electron creation operators, with $c_{i\sigma}$ and $d_{i,\sigma}$ the operators for O and TM orbitals, respectively, with the convention that ith TM atom is placed to the left of the ith O atom. As usual, $n_{d,i,\sigma} = d^\dagger_{i\sigma}d_{i\sigma}, n_{i\sigma} = c^\dagger_{i\sigma}c_{i\sigma}$. For book-keeping purposes we assume that there are N TM and N O sites, but in the final calculation we let $N\to\infty$. We also assume that only the $2p$ O orbitals pointing towards the TM neighbors are relevant to the calculation. Generalization to models that include more O and/or TM orbitals, as well as lattices in higher dimensions, are discussed below.

For AES in a system with full bands, we start from the completely full ground state $|\Omega\rangle_P = \prod_{i,\sigma} d^\dagger_{i,\sigma}c^\dagger_{i,\sigma}|0\rangle$ of energy $E^P_\Omega = N(2\Delta + U + U_O)$, and create two holes. Because the periodic Hamiltonian is invariant to translations and because we want to describe states where the two holes could be at the same TM site, we choose two-hole basis states with a total momentum k and zero spin projection,[25] namely $|k,n,dd\rangle = \frac{1}{\sqrt{N}}\sum_i e^{ik(R_i+na/2)}d_{i,\uparrow}d_{i+n,\downarrow}|\Omega\rangle_P$ if both holes are on TM sites, $|k,n,dc\rangle = \frac{1}{\sqrt{N}}\sum_i e^{ik(R_i+na/2)}d_{i,\uparrow}c_{i+n,\downarrow}|\Omega\rangle_P$ and $|k,n,cd\rangle = \frac{1}{\sqrt{N}}\sum_i e^{ik(R_i+na/2)}c_{i,\uparrow}d_{i+n,\downarrow}|\Omega\rangle_P$ if one hole is on a TM site and the other is at an O site, and finally $|k,n,cc\rangle = \frac{1}{\sqrt{N}}\sum_i e^{ik(R_i+na/2)}c_{i,\uparrow}c_{i+n,\downarrow}|\Omega\rangle_P$ if both holes are in the O bath. Here a is the lattice constant and $n = -\frac{N}{2}+1,\ldots,\frac{N}{2}$ takes all possible values consistent with the periodic boundary conditions. Taken together, these states constitute a full basis for the Hilbert subspace containing states with total momentum k and zero spin projection.

The aim is to find the propagator

$$G_{dd}(k,0,\omega) = \langle k,0,dd|\hat{G}_P(\omega)|k,0,dd\rangle$$

where $\hat{G}_P(\omega) = [\omega + i\eta - (\mathcal{H}_{\mathcal{P}} - E^P_\Omega)]^{-1}$ is the resolvent for $\mathcal{H}_P$, because its associated spectral weight $A_{dd}(k,0,\omega) = -\frac{1}{\pi}{\rm Im}[G_{dd}(k,0,\omega)]$, which has poles at energies $\omega = E_{2h}(k) - E^P_\Omega$ for any two-hole eigenstate with total momentum k and energy $E_{2h}(k)$, is proportional to the momentum-resolved spectral intensity measured by AES. As discussed below, our solution also provides the values of many other propagators beside $G_{dd}(k,0,\omega)$, from which other useful information can be gleaned.

B. Anderson impurity problem

We reduce the full periodic problem to the Anderson impurity problem sketched in Fig. 1(b), by simplifying the Hamiltonian to:

$$\mathcal{H}_I = \mathcal{H}_{\rm TM,I} + \mathcal{H}_{\rm O} + \mathcal{H}_{\rm hyb,I}$$

where

$$\mathcal{H}_{\rm TM,I} = Un_{d,\uparrow}n_{d,\downarrow} + \Delta\sum_\sigma n_{d,\sigma}$$

describes the impurity TM site, the O bath is described by $\mathcal{H}_{\rm O}$ as before, and

$$H_{\rm hyb,I} = -V\sum_\sigma[d^\dagger_\sigma c_{1,\sigma} + d^\dagger_\sigma c_{0,\sigma} + h.c.]$$

is their hybridization, with the impurity taken to be located between the bath O labeled '0' and '1'. Here, again, all operators are electron operators and $d_\sigma^\dagger$ is the creation operator for the orbital of the TM impurity site.

The filled-band ground state is now $|\Omega\rangle_I = \prod_\sigma d_\sigma^\dagger \prod_i c_{i,\sigma}^\dagger |0\rangle$ and its corresponding energy is $E_\Omega^I = 2\Delta + U + NU_0$. To calculate AES-relevant spectra we consider two-hole excitations in this ground state by removing two electrons with opposite spins. Since invariance to translations is lost, the generic real space states of interest are now $|i\sigma, j\sigma'\rangle \equiv c_{i\sigma}c_{j\sigma'}|\Omega\rangle_I$, $|d\sigma, i\sigma'\rangle = d_\sigma c_{i\sigma'}|\Omega\rangle_I$ and $|dd\rangle = d_\uparrow d_\downarrow |\Omega\rangle_I$. Now we are primarily interested in calculating the two-hole impurity Green's function $G_{dd}(\omega) = \langle dd|\hat{G}_I(\omega)|dd\rangle$ where $\hat{G}_I(\omega) = [\omega + i\eta - (\mathcal{H}_\mathcal{I} - E_\Omega^I)]^{-1}$, and its corresponding two-hole spectral function $A_{dd}(\omega) = -\frac{1}{\pi}\mathrm{Im}[G_{dd}(\omega)]$.

III. METHOD

We begin with the exact solution for the periodic Anderson model. To find the propagator of interest to us, $G_{dd}(k, 0, \omega)$, we generate its equation of motion (EOM) from the identity: $\hat{G}_P(\omega)(\omega - \mathcal{H}_P + E_\Omega^P + i\eta) = \hat{I}$. Calculating its diagonal matrix element for $|k, 0, dd\rangle$, we find:

$$(\omega + 2\Delta + U + i\eta)G_{dd}(k,0,\omega) = 1 + V\left[e^{\frac{ika}{2}}G_{cd}(k,1,\omega) + G_{cd}(k,0,\omega) + e^{\frac{ika}{2}}G_{dc}(k,-1,\omega) + G_{dc}(k,0,\omega)\right]$$

where $G_{\alpha\beta}(k, n, \omega) = \langle k, 0, dd|\hat{G}_P(\omega)|k, n, \alpha\beta\rangle$ for $\alpha, \beta = c, d$. In other words, because the Hamiltonian links the state $|k, 0, dd\rangle$ to states with one hole on a TM site and one on a neighboring O, the EOM links $G_{dd}(k, 0, \omega)$ to propagators corresponding to such states. Their EOM can be generated similarly, and we obtain an infinite sequence of coupled linear equations.

To solve it, we couple the propagators with holes at the same distance n in a vector:

$$V_n = \begin{pmatrix} G_{dd}(k,n,\omega) \\ G_{dc}(k,n,\omega) \\ G_{cd}(k,n,\omega) \\ G_{cc}(k,n,\omega) \end{pmatrix}$$

and note that for any $n \neq 0$, the EOM can be grouped in the simple recurrence relation:

$$\gamma_n V_n = \beta_n V_{n+1} + \alpha_n V_{n-1}$$

for any given k and ω. Here γ_n, β_n and α_n are simple 4×4 matrices that are read off directly from the EOM. We note that one can always group the EOM in such simple recurrence relations, even for models which allow longer-range hopping[26] and/or in higher dimensions.[27] For $n = 0$, the recurrence relation also has an inhomogeneous term:

$$\gamma_0 V_0 = X + \beta_0 V_1 + \alpha_0 V_{-1},$$

where $X^T = (1, 0, 0, 0)$ for this problem. The solution of such recurrence relations has been discussed extensively elsewhere.[25–27] Briefly, we must have $V_n \to 0$ as $|n| \to \infty$, because the Fourier transform of these propagators are the amplitudes of probability to have the two holes evolve from being on the same TM site to being n sites away from each other, in a given time. As $|n| \to \infty$ this becomes very unlikely, and the presence of the broadening η which introduces an artificial lifetime $1/\eta$ makes it even less so. As a result, for $n \geq 1$ we have $V_n = A_n(k, \omega)V_{n-1}$ where $A_n = [\gamma_n - \beta_n A_{n+1}]^{-1}\alpha_n$ is calculated starting with $A_M = 0$ for a sufficiently large cutoff M. Similarly, for $n \leq -1$ we have $V_n = B_n(k, \omega)V_{n+1}$ where $B_n = [\gamma_n - \alpha_n A_{n-1}]^{-1}\beta_n$ is calculated starting with $B_{-|M|} = 0$. Using $V_1 = A_1 V_0$ and $V_{-1} = B_{-1}V_0$ in the $n = 0$ equation gives:

$$V_0 = [\gamma_0 - \beta_0 A_1(k,\omega) - \alpha_0 B_{-1}(k,\omega)]^{-1} X.$$

This gives us $G_{dd}(k, 0, \omega)$ as the top entry in V_0. All other $n = 0$ propagators, as well as those with $|n| < M$, can also be then calculated efficiently. Projecting on a different state than $\langle k, 0, dd|$ also simply requires using a different X, so other propagators can also be found easily with this scheme.

In principle, this method generalizes straightforwardly to lattices in any dimension and with any topology, so no approximations should be necessary. In practice, however, the computational cost quickly becomes prohibitive. For instance, for models with nearest-neighbor hopping in higher dimensions, one must group together in V_n all propagators where the holes are separated by $n_x a\hat{e}_x + n_y a\hat{e}_y + \dots$ with $|n_x| + |n_y| + \dots = n$, i.e. with the same Manhattan distance.[27] As a result, the dimension of V_n increase roughly like n^{d-1}. Adding more orbitals at the TM/O sites will further amplify the problem, by increasing in a combinatorial fashion the number of possible propagators with the same $(n_x, n_y, \dots)$ separation. As a result, while the solution can still be cast in terms of continued fractions of matrices, their dimensions increase fast with n resulting in significant computational costs. This is why efficient approximations are needed.

As already mentioned, one much-employed option is the impurity approximation. Its solution for $G_{dd}(\omega)$ can also be formulated in terms of continued fractions of matrices (we present the details in the Appendix, since we are not aware of a prior similar solution for this prob-

lem). This approximation reduces the number of possible propagators by removing all but one TM site from the problem. As a result, there is now only one state with both holes at the impurity TM site as opposed to N^2 in the full periodic problem (i.e., including all allowed total momenta), and only $2N$ combinations with one hole at the TM and one at an O site, as opposed to $2N^2$ options in the full problem. The number of states associated with both holes in the O bath is not changed.

The total number of distinct propagators is therefore reduced from $4N^2$ in the full problem to $(N+1)^2$ in the impurity limit, suggesting that the latter is considerably more efficient. However, the full problem can be solved individually for each of the allowed N total momenta, since the translational invariance guarantees that propagators with different momenta do not mix. Thus, one needs to solve N distinct problems with $4N$ propagators each, as discussed above. In the impurity problem, loss of translational invariance means that all propagators are coupled to one another through the EOM. From this perspective, it is far less clear that using the impurity approximation is computationally more efficient, although to fully settle this one needs to take into account of all other possible symmetries and the effects of the truncation (for large system, the cutoff $M \ll N/2$). In practice the O bath is often replaced by a featureless density of states (we do not make this further approximation in our calculations). This certainly makes the impurity problem very efficient, but it also looses all information regarding the role of the O bath topology, on top of the loss of ability to momentum-resolve the AES spectral weights.

From this analysis, it is clear that a better strategy would be to lower the total number of propagators while maintaining translational invariance. This is the basis for our proposed variational method. Our proposal is to remove the propagators which have the holes at different TM sites. This is equivalent with excluding these states from the Hilbert space, which is why this is a variational approximation. Mathematically, this is easily achieved by setting $G_{dd}(k,n,\omega) \equiv 0$ for all $n \neq 0$ in the EOM discussed above, leading to vectors V_n, $n \neq 0$ of dimension 3 instead of 4. Of course, the saving is not big for this simple problem, but it starts to become considerable in higher dimensions and/or for more TM/O orbitals.

Physically, what this means is that both holes start at the same (any) TM site. Eventually both may hop into the O bath and move through the system, but whenever they happen to hop back to TM sites they must both go to the same TM ion. For systems with strong correlations, i.e. where the states with the holes at the same TM site are at quite different energies from states with the holes as different TM sites, this should be a reasonable approach and is close to the intuitive picture of what happens in AES. In a way, one could view this as a "lattice of impurities". Besides maintaining translational invariance, this variational approximation has the added benefit that we can infer apriorily the effect of removing these states, as we discuss in the next section. Moreover, if need be one can also systematically add some of these states back into the calculation – for example, starting with the states where the holes belong to neighboring TM sites only. Their importance can therefore be assessed quantitatively. Generalization to systems with partially filled TM orbitals is also much less computationally costly than for the full solution. More discussion on the meaning and relevance of this approximation is presented below, as we discuss its predictions.

IV. RESULTS

A. The periodic Anderson model

We start by discussing the full periodic model. Besides providing the test case against which we compare the variational and the impurity approximations, this also allows us to understand the various features of these spectra and their dependence on the various parameters. Since the phenomenology which leads to the appearance of these various features is general, qualitatively similar spectra should be expected in more complex systems.

To understand the dependence of the AES spectral weight with both holes at the same the TM site, $A_{dd}(k,0,\omega)$, on the various parameters, we start by setting $U = U_O = 0$, $t = V = 1$, and varying Δ. Momentum-resolved results are shown in Fig. 2 for uniformly spaced values of k from 0 and π/a.

To make sense of these fairly complicated spectra, we note that these parameters correspond to a non-interacting system. As a result, the two-hole spectra must be convolutions of single-hole spectra, which are easy to calculate for this simple model (note that single-hole spectra can also be obtained experimentally from Angle-Resolved Photoemission). Straightforward calculations shows that a hole of momentum k introduced in the state $|\Omega\rangle_P$ has two possible eigenenergies:

$$E_{1h}^{(\pm)}(k) = \frac{1}{2}\left[-U-\Delta-U_O+2t\cos(ka) \pm \sqrt{\left(U+\Delta-U_O+2t\cos(ka)\right)^2+16V^2\cos^2\frac{ka}{2}}\right]. \quad (1)$$

Roughly speaking, these correspond to either having the hole preponderantly on the TM sites (i.e., a TM-like

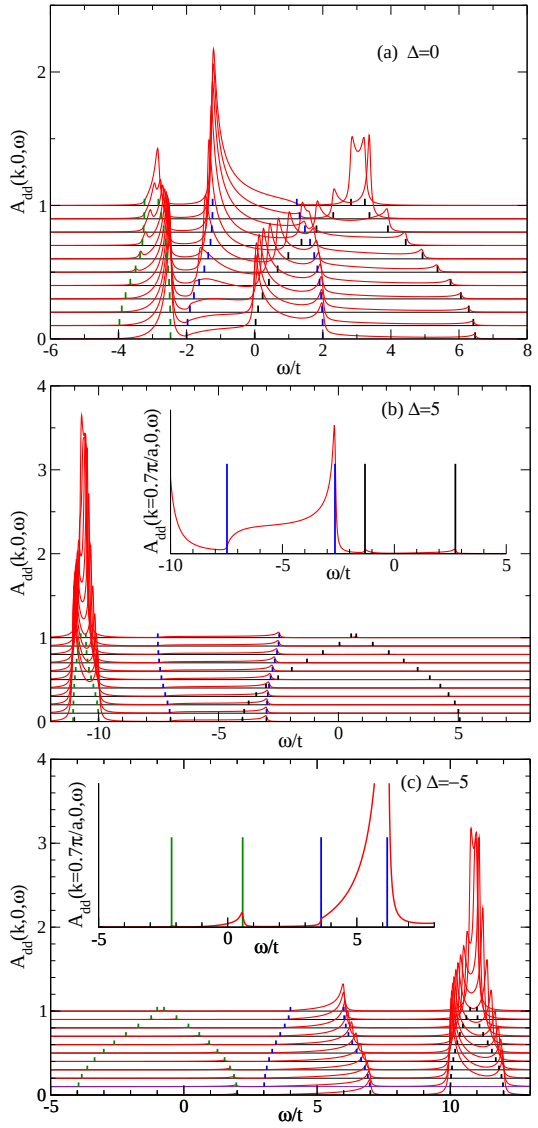

FIG. 2. (color online). AES spectral weights $A_{dd}(k,0,\omega)$ for the full periodic model vs. ω for $k \in [0,\pi/a]$. The curves are shifted vertically with increasing k. In all cases $t = V = 1, U = U_0 = 0, \eta = 0.05$, while (a) $\Delta = 0$; (b) $\Delta = 5$; (c) $\Delta = -5$. The small vertical lines indicated the expected locations of band edges. See text for more details.

band) or in a O-like band. Note that the electron correlations energies U, U_0 enter here because the single hole is introduced in an otherwise full band.

The convolution of these two one-hole continua result in three two-hole continua, covering the ranges $E_{2h}^{(\gamma\delta)}(k) \in \{E_{1h}^{(\gamma)}(k-q) + E_{1h}^{(\delta)}(q)| - \frac{\pi}{a} < q \leq \frac{\pi}{a}\}$ for $\delta, \gamma = \pm$. Their band edges are shown by small vertical markers in Fig. 2; each band has a different color. These expected band-edges indeed agree perfectly with the features seen in the AES spectral weight (a broadening $\eta = 0.05$ was used in the spectral weight, accounting for the apparent "overflow").

For $\Delta = 0$, the two upper bands overlap partially,

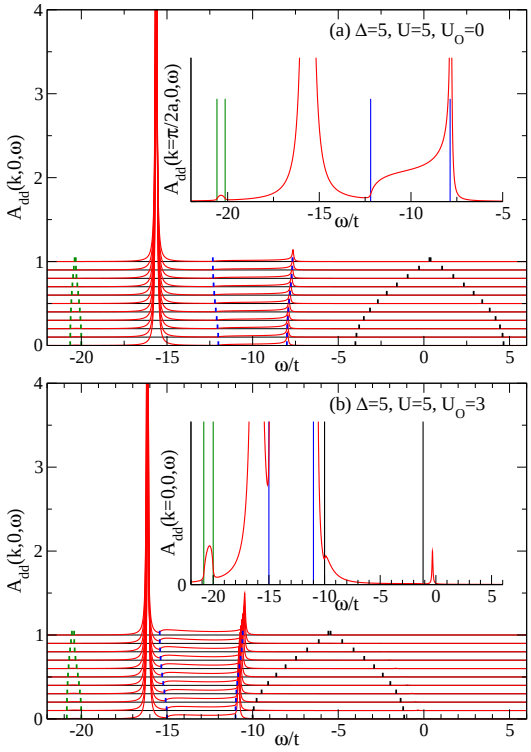

FIG. 3. (color online). AES spectral weights for the full periodic model $A_{dd}(k,0,\omega)$ vs. ω for $k \in [0,\pi/a]$. The curves are shifted vertically with increasing k. In all cases $t = V = 1, \Delta = 5, \eta = 0.05$, while (a) $U = 5, U_O = 0$; (b) $U = 5, U_O = 3$. The small vertical lines indicated the expected locations of band edges. See text for more details.

and the spectral weight is distributed fairly equally between all features. For $\Delta = \pm 5$, most of the weight is in the lowest/highest continuum which contains states with both holes in the TM-like band and thus has the highest overlap with the state $|k,0,dd\rangle$ of interest to AES. This band is centered at -2Δ, which is the change in energy if two holes are removed from TM sites if there was no hybridization, $V = 0$, and in the absence of correlations $U = U_0 = 0$, and is fairly narrow since the holes cannot hop directly between TM sites. The middle continuum, with one hole in the TM-like band and one in the O-like band, has less weight but is still visible. It is centered around $-\Delta$, i.e. the energy cost for removing one electron from the TM site, and is broader because the O-like band has significant bandwidth. The third continuum, with both holes in the O-like band, has very little overlap with the state $|k,0,dd\rangle$ and is therefore only visible when the scale is significantly expanded, as shown in the insets. It is centered around the origin (for $U_0 = 0$) and is the broadest of the three features because holes can hop directly between O sites. In the limit $V \to 0$, the maximum bandwidth of this continuum should be $8t$, when $k = 0$. We see that hopping to and off the TM sites, controlled by V, can have a significant influence on this value when $V \sim t$.

While one can set any values for parameters in a theoretical study, physically it makes sense to focus on cases where the low-energy states favor having the extra holes at the TM sites, so that AES is maximally sensitive to the TM parameters. Simple arguments, listed in Appendix B, show that this implies $\Delta > 2t + U_O$.

As a result, we set $\Delta = 5$ and investigate the role of the on-site correlations. Fig. 3(a) shows $A_{dd}(k, 0, \omega)$ for $U = 5, U_O = 0$ while Fig. 3(b) is for $U = 5, U_O = 3$. Comparing Fig. 3(a) with Fig. 2(b), we see that the lowest band with the two holes in the TM-like bands has shifted by about $2U$ and is now centered around $-2(\Delta + U)$, as expected since $-(\Delta + U)$ is the energy cost for removing an electron from a TM site (if there was no hybridization with the O bath). Similarly, the middle band is shifted by about U to around $-\Delta - U$, while the upper band with the two holes in the O bath is essentially unchanged. Apart from these expected shifts, we see that most spectral weight has moved from the lowest band (where it was for $U = 0$) into a new discrete peak that has appeared $\sim U$ above it. This weakly dispersing peak describes (anti)bound states with both holes at the same TM site, hence the large overlap with $|k, 0, dd\rangle$. Indeed, it is located close to $-2\Delta - U$, where it would be expected to appear in the absence of hybridization with the O bath. For our simple model, this peak represents the "multiplet structure" associated with the TM element. For a more realistic calculation, for example for Cu_2O, this peak would be replaced by the atomic-like multiplet structure of the Cu as seen in experiments.[6]

Correlations at the O site have similar effects, as shown in Fig. 3(b). Since the cost of removing an electron from the O ion is now lowered by U_O, the central band shifts by an additional $-U_O$ while the upper band shifts by an additional $-2U_O$. On the other hand, the lowest band with the two holes in the TM-like band is essentially unchanged, while the "multiplet" peak is shifted to slightly lower energies due to level repulsion with the central continuum. Correlations at O sites also produce an (anti)-bound discrete state with both holes at the same O site which is pushed above the upper continuum. However, it has very little weight and can only be seen on a greatly expanded scale, as shown in the inset, as a small peak located just above the highest-energy bandedge.

To summarize, the location of the continua in the momentum-resolved AES spectrum must agree with the convolution of the one-hole spectra, which can be obtained from ARPES. Additional discrete peaks (or strong sharp resonances, if these happen to fall inside another continuum) indicate the presence of on-site correlations, and allow one to find various on-site parameters from the corresponding multiplet structure. Of course, because the projection is on the $|k, 0, dd\rangle$ state, the spectral weight is large for states which predominantly have both holes at the same TM site. As discussed in the previous section, it is trivial with our method to project on other states, for example with both holes at the same O site. While the spectrum is unchanged, this will shift the spectral weight between the different features.

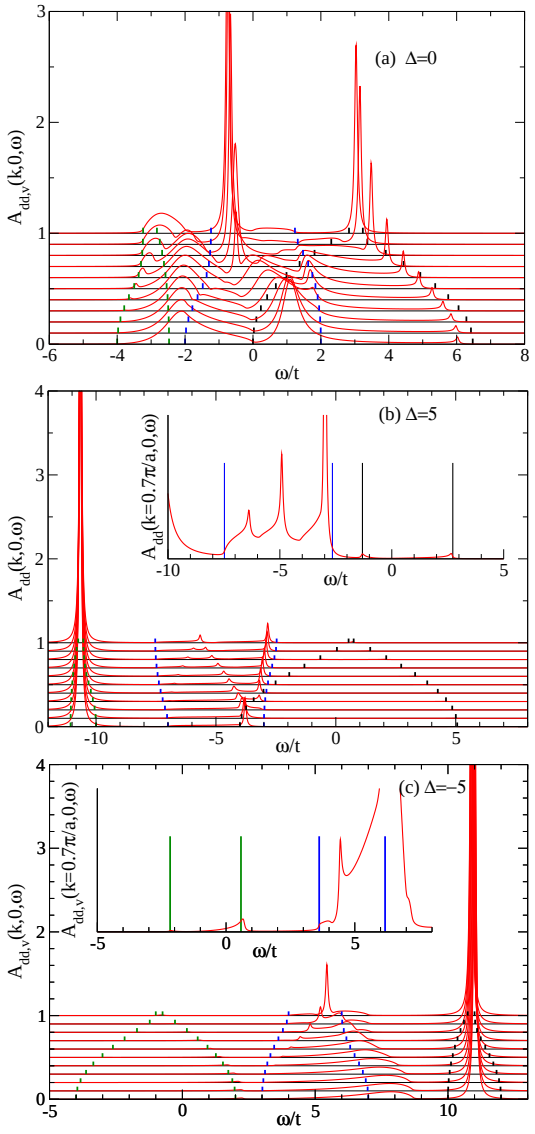

FIG. 4. (color online). Same as in Fig. 2, but the AES spectral weight is obtained with the variational approximation.

B. Variational approximation

We now present data obtained with our variational approximation for the same sets of parameters, in Figs. 4 and 5. As before, the vertical markers show the expected location of the band-edges, based on the convolution of the one-hole spectra.

Starting with the un-correlated case in Fig. 4, we see that this variational approximation is very poor when $\Delta = 0$, in panel (a). While the overall spectral range is in fair agreement with that predicted by the two-hole convolutions, inside this interval there is significant disagreement. In particular, the variational calculation predicts spectral weight at energies that should be gaped.

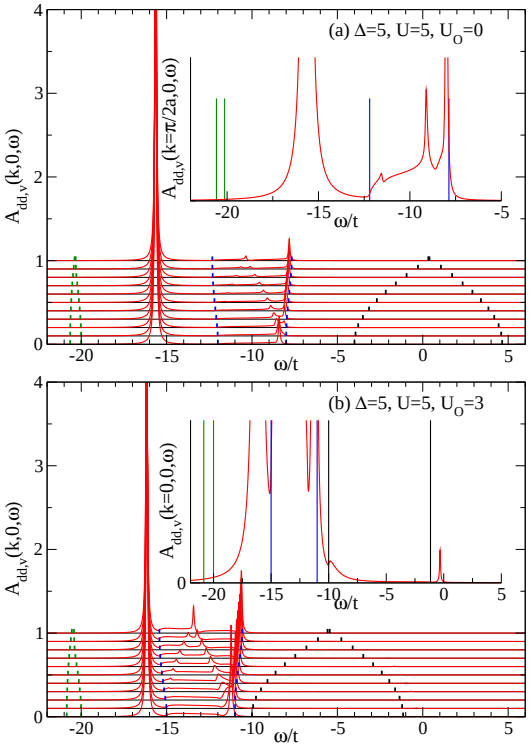

FIG. 5. (color online). Same as in Fig. 3, but the AES spectral weight is obtained with the variational approximation.

This disagreement is not surprising, since in this case we are projecting out states that have energies very similar to the states we keep, and this is not a sensible strategy.

As shown in panels (b) and (c), the situation improves when Δ is large enough to separate the TM-like band from the O-like band. In this case, the agreement for the two less visible bands is reasonable, even though the projection may slightly over/underestimate the location of the band-edges and it certainly produces additional structure within the bands, especially the central one. This is not surprising since one expects a fair amount of hybridization between states in the central continuum, which have one hole in the TM-like band and one in the O-like band, with the states with the two holes at different TM sites that are projected out.

Finally, the continuum with the two holes in the TM-like bands is replaced by discrete peaks located at roughly the correct energy. The disappearance of this continuum is expected, since we projected out precisely the states responsible for generating it, i.e. with holes at different TM sites. In the absence of correlations, the state with both holes at the same TM site has a similar energy, hence the peak. Similar conclusions hold for $\Delta = -5$.

If we turn on the correlations, this "multiplet structure" peak moves away from the continuum. Indeed, as shown in both panels of Fig. 5, now the low-energy continuum with the two holes in the TM-like band is completely absent from the variational results but the important feature, i.e. the high-weight "multiplet structure"

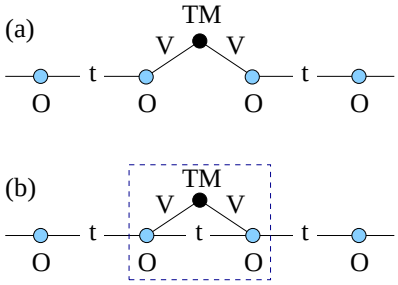

FIG. 6. Two ways to connect the impurity to the O bath: (a) trivial, and (b) non-trivial topology. The latter can be reduced to the former if one considers the three central ions enclosed by the box to form an effective "impurity".

peak, is essentially indistinguishable from that predicted by the full solution. The higher energy continua show some additional structure within this variational calculation, but since this structure also appears in the absence of correlations there is little danger of confusing it with real features induced by the correlations.

To summarize, for parameters likely relevant for the real materials, i.e. when the TM-like and O-like bands are sufficiently well separated, the variational approximation does a very good job in capturing the multiplet structure due to TM on-site correlations. One of the continua is projected out, but it has little weight and its location is apriorily known from the one-hole spectrum. The higher energy continua are reproduced at roughly the correct locations but with some additional features, which however also appear in the absence of correlations. With some care, one can use this more efficient calculation to understand most, if not all, the important physics contained within these spectra.

C. Impurity approximation

For comparison, we also present AES spectra obtained with the impurity approximation. Since here the translational invariance is lost, we can only show one $A_{dd}(\omega)$ curve for each set of parameters. This can be roughly thought of as a momentum-integrated spectral weight.

We begin by considering the simpler impurity model sketched in Fig. 6(a), where the TM impurity is connected to two independent semi-infinite half chains. The reasons for studying this case first are that (i) it is simpler to understand the resulting AES spectrum; (ii) one can think of the actual case of interest, shown in Fig. 6(b), as a generalization of this case, by treating the 3 central atoms enclosed in the box as an effective impurity with a more complicated level structure, but which is otherwise connected to two independent semi-infinite half chains; (c) comparison between these two cases will reveal whether the particular way in which the impurity connects to the O bath plays a significant role.

Fig. 7 shows results for several sets of parameters. In

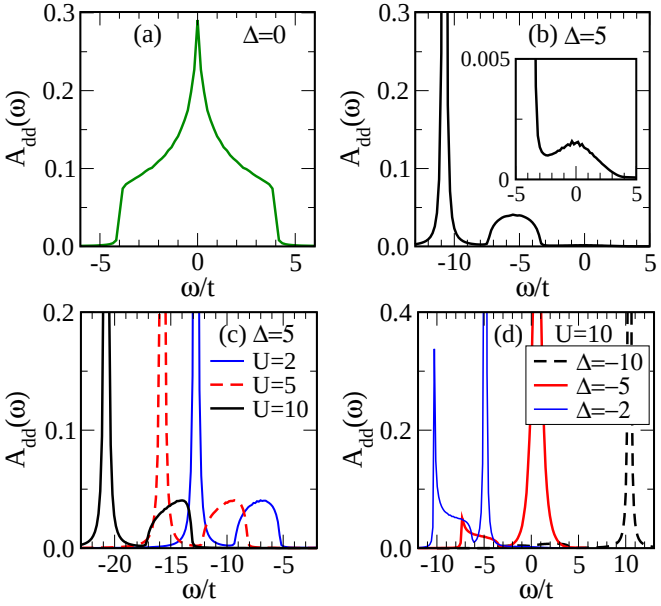

FIG. 7. (color online). Impurity spectral function $A_{dd}(\omega)$ vs. ω for the trivial topology of Fig. 6(a) with $t = V = 1$ and (a) $\Delta = U = U_O = 0$, (b) $\Delta = 5, U = U_O = 0$. The inset shows the two-hole continuum on an expanded scale. (c) $\Delta = 5, U = 2, 5, 10, U_O = 0$, and (d) $\Delta = -10, -5, 2, U = 5, U_O = 0$.

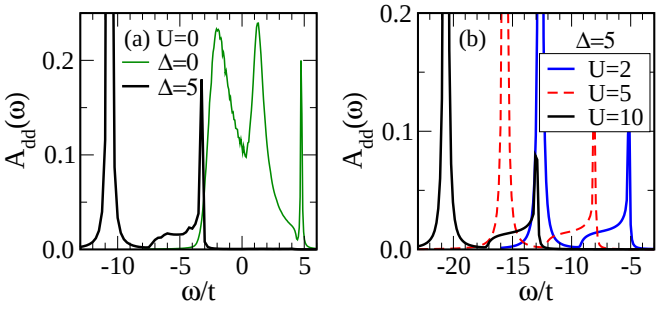

FIG. 8. (color online). Impurity spectral function $A_{dd}(\omega)$ vs. ω for the non-trivial topology of Fig. 6(b) with $t = V = 1$ and (a) $\Delta = 0, 5$ and $U = U_O = 0$, (b) $\Delta = 5, U = 2, 5, 10, U_O = 0$.

all cases $t = V = 1$. Panel (a) shows the case $\Delta = U = U_O = 0$. Since there is now no difference between the TM and the O sites, this describes two independent holes on an infinite chain with nn hopping. The spectral weight has the expected shape for this problem, with the two-hole convolution continuum ranging from $[-4t, 4t]$. This is quite different from the exact result in this limit, shown in Fig. 2a.

In all the other panels $\Delta \neq 0$ so that the single hole spectrum consists of the O band and a TM-like impurity state. As a result, the 2-holes convolution consists of three features. The first is a discrete state which primarily has both holes at the TM site. In the absence of hybridization ($V = 0$), this feature is located at $-2\Delta - U$ and represents the "multiplet" of primary interest. The second feature is a one-hole continuum describing states with one hole occupying the TM impurity state and the other moving freely in the O bath. This replaces the continuum with one hole in the TM-like band and one in the O-like band, from the exact and the variational solutions. In the absence of hybridization, this feature extends over $[-\Delta - U - U_O - 2t, -\Delta - U - U_O + 2t]$. Finally, the third feature is a two-hole continuum with both holes in the O bath. This corresponds to the continuum with both holes in the O-like band, but here it spans the interval $[-2U_O - 4t, -2U_O + 4t]$ irrespective of the value of V.

The results in panels (b)-(d) of Fig. 7 agree with these expectations. Like in the full calculation, the continuum with the holes in the O bath has very little weight and can only be seen on an expanded scale, if $\Delta \neq 0$. The one-hole continuum is at the expected location, while the discrete peak is slightly shifted through level repulsion.

Results for similar parameters, but for the non-trivial topology of Fig. 6(b), are shown in Fig. 8. Here the impurity forms a ring with its two neighbor O sites. The main difference is that the more complex "ring impurity" has more internal eigenstates, and these do not hybridize equally with the bath. For example, while there is a single eigenstates with one hole at the TM site, the isolated 3-site ring has 3 eigenstates with one hole on the ring. Two of these eigenstates involve the TM site (the third is the anti-symmetric combination of the O sites so it is a bath state). As a result, here we expect two one-hole continua in the AES two-hole spectrum, corresponding to states having one hole in one of these two ring eigenstates, and the second in the O bath. Similarly, while the TM atom has a single two-hole eigenstates, the 3-site ring has four such eigenstates in the $S_z = 0$ sector. If $U_O = 0$, only 3 of these involve the TM site, the fourth one is a bath state. As a result, for $U_O = 0$ we should expect to see 3 peaks marking this "multiplet".

A summary of the results is shown in Fig. 8. In panel (a), we plot $A_{dd}(\omega)$ for $t = V = 1, U = U_O = 0$ and $\Delta = 0, 5$. The $\Delta = 0$ case (thin green line) looks very different from its counterpart in Fig. 7(a): the two-hole continuum is located between $[-4t, 4t]$, as expected, but it has two broad resonances and there is a discrete peak just above it. This can be easily understood in terms of the ring "multiplet". For these parameters, the isolated ring supports three distinct two-hole eigenstates, with energies $-2t, t, 4t$. The two broad resonances are clearly associated with the former two. The third peak falls right at the two-hole continuum's upper edge, and level repulsion pushes it just above the band-edge. The one-hole continua overlap with the two-hole continuum, for these parameters, so they are not visible.

For $\Delta = 5$ (thick black line), the spectrum is rather similar to that shown in Fig. 7(b), despite the different topology. The reason is that for these parameters, the 3 two-hole ring eigenstates are at $-10.63t, -4t, 2.63t$. The latter two fall inside the two-hole continuum, so only the former is expected to be visible. The result confirms this expectation. Similarly, the 2 one-hole ring eigenstates are at $-5.32t, 1.32t$ and should result in one-hole con-

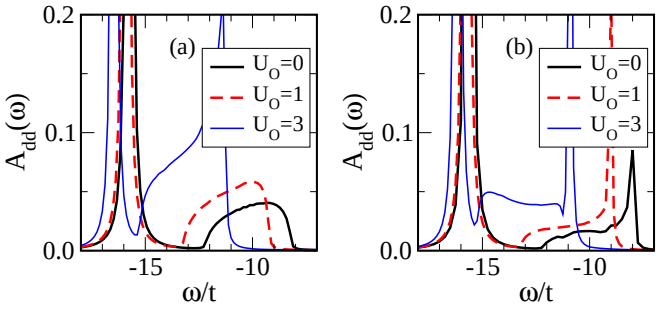

FIG. 9. (color online). Impurity spectral function $A_{d\uparrow,d\downarrow}(\omega)$ vs. ω for (a) the trivial topology and (b) the ring topology, with $t = V = 1, \Delta = U = 5$ and $U_O = 0, 1, 3$.

tinua spanning $[-7.32t, -3.32t]$ and $[-0.68t, 3.32t]$, respectively. Again, only the former is (partially) distinct from the two-hole continuum, and indeed it is clearly visible in the spectrum. Thus, even though the multiplet structure is more complex for the ring topology, the results do look quite similar to those for the trivial topology as most of the additional features fall inside the two-hole continuum.

Similar conclusions are valid when we turn on the correlations, as shown in panel (b). The results are again qualitatively like those for the trivial topology, because the additional states in the ring multiplet fall inside the two-hole continuum and are washed out into broad, low-weight resonances. This is certainly true for $U \gg t, |\Delta| \gg t$, when the TM states become (to zero order in perturbation theory) eigenstates of the ring, with the remaining ring eigenstates involving only O sites and therefore being located inside the two-hole continuum. For finite values of U and Δ there are quantitative differences in the precise location of various features and in the shape of the continua.

Finally, in Fig. 9 we briefly discuss the effect of the on-site repulsion at the O sites in the impurity approximation. Panel (a) is for the trivial topology while panel (b) is for the ring topology. In both cases, $t = V = 1, U = \Delta = 5$, and three values $U_0 = 0, 1, 3$ are shown. In the trivial topology, the main effect of U_0 is to shift the one-hole continuum to lower energies by U_0, as expected. This leads to a stronger hybridization with the discrete peak, which is consequently pushed to lower energies as well. The weights in these features also very somewhat, except for the two-hole continuum which remains invisible on this scale. For these parameters, the results for both topologies are qualitatively similar for reasons explained above.

To summarize, we find that the results for the two topologies are rather similar if $|\Delta|$ and/or U are large compared to t, V. If this is not the case their predictions can be quite different, however in such cases the impurity approximation itself becomes very suspect.

When valid, the impurity approximation is fairly successful in reproducing the location of the multiplet peak, as shown in Fig. 10 where we compare $A_{dd}(\omega)$ for the trivial topology (dot-dashed line) against $\frac{1}{N}\sum_k A_{dd}(k,\omega)$ for the exact solution (full line) and our variational approximation (dashed line), for $\Delta = U = 5, U_O = 0$. The multiplet peak disperses very weakly for these parameters so all three curves show what looks like a discrete peak at low energies. The impurity approximation is less successful in predicting the correct bandwidth for the continuum visible at higher energies; when analysing experimental data, this may result in wrong values assigned to the hopping parameters. In any event, Fig. 10 confirms again that our variational approximation is more accurate than the impurity approximation even for this simplest possible problem.

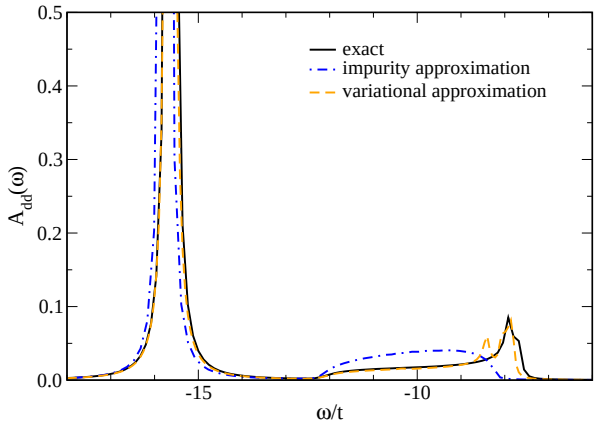

FIG. 10. Momentum integrated AES spectral weight $\frac{1}{N}\sum_k A_{dd}(k,\omega)$ for the exact solution (full line) and our variational approximation (dashed line) compared to the prediction of the impurity approximation with trivial topology (dot-dashed line), for $t = V = 1, U = \Delta = 5, U_O = 0$.

V. DISCUSSION & CONCLUSIONS

In this work we introduced a novel variational approach to calculate two-particle Green's functions needed for AES spectroscopy. Here we applied it to a simple 1D model with otherwise full bands, so that we can compare its predictions against the exact solution available for this case. We also calculated the results in the impurity approximation, for two different ways of connecting the impurity to the O bath.

Both approximations are reasonable to use only if the single-electron parameters are such that one-hole eigestates with the hole primarily at the TM site (i.e., of TM character) are energetically well separated from those with the hole primarily in the O band. If this is not true, then the basis states projected out in these approximations are energetically close to those kept within the calculation, and the results are not sensible.

If this condition is satisfied, we believe that these results clearly show that our variational approximation is superior to the impurity approximation. Not only does it

produce momentum-resolved results, but the location of the continua that appear in the AES spectrum is in fair agreement with that expected from the convolution of the one-hole spectrum, unlike for the impurity approximation. Since the one-hole spectrum can be obtained from ARPES measurements (and, from a theoretical perspective, can be calculated with methods analogous to those we use here to find the two-hole propagator), a combination of the two spectroscopies can be used to determine which features in the two-hole spectrum come from this convolution. Any other features must be due to on-site correlations, and can therefore help pinpoint the values of various on-site interaction energies.

The method of Ref. 25 can be extended straightforwardly to compute Green's functions for problems with three or more holes, which would be relevant for AES is systems with partially filled bands, because the resulting equations of motion can still be grouped into simple recurrence relations. In practice, a variational approximations along the lines we proposed here will significantly decrease the computational cost while removing from the spectrum only low-weight features whose location can be inferred apriorily from knowledge of the one-hole spectra, as already discussed. This opens an efficient way to make progress on understanding AES spectra for systems where the d orbitals of the TM are only partially filled, so long as the states of TM character are not too close to the O character states. Such work is now in progress.

ACKNOWLEDGMENTS

This work was supported by NSERC, CIfAR and QMI.

Appendix A: Continued-fraction solution for the impurity approximation

Since we lose the translation invariance, here we have to work explicitly in the real space. In the following we generalize the continued-fraction approach to the Anderson impurity problem.

For technical reasons which will become apparent soon, it is more convenient to group the TM together with the two O sites it directly hybridizes with into "site" 0, and to index the O atoms to its right/left as $\pm1, \pm2$, etc. The two O inside "site" 0 will be called "a" and "b", respectively. This indexing is shown in Fig. 11. Amongst other things, this indexing makes it easy to study the two situations depicted in Figs. 11(a) and (b), where the hopping between the two central O is turned off/on.

We use the operator identity $(\omega + E^I_\Omega + i\eta - \mathcal{H}_\mathcal{I})\hat{G}_I(\omega) = \hat{I}$ to generate EOMs for the Green's functions. For example, for any $|i| > 1, |j| > 1$, this results in: $(\omega + E^I_\Omega + U_O(2-\delta_{i,j}) + i\eta)G_{i\uparrow,j\downarrow}(\omega) = tG_{i\uparrow,j+1\downarrow}(\omega) + tG_{i-1\uparrow,j\downarrow}(\omega) + tG_{i\uparrow,j-1\downarrow}(\omega) + tG_{i+1\uparrow,j\downarrow}(\omega)$, where $G_{i\sigma,j\sigma'}(\omega) = \langle dd|\hat{G}_I(\omega)|i\sigma, j\sigma'\rangle$. In other words, it

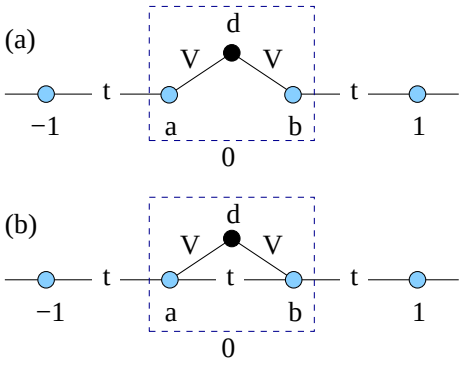

FIG. 11. Actual indexing of the O sites used in this work. The three central atoms comprise "site" 0.

links together propagators where the holes are at a distance $|i-j| = n$ apart, to propagators where the holes are $n\pm1$ sites apart. This allows us to rewrite these equations of motion as simple recurrence relations by grouping together in a vector V_n all the propagators where the holes are n sites apart. Note that this is true for states with a hole at "site" 0 and one at any site $|n| \geq 1$, which also enter into V_n and only link to propagators in $V_{n\pm1}$.

To be more precise, let:

$$V_n^{\sigma,\sigma'} = \begin{pmatrix} \cdot \\ \cdot \\ \cdot \\ G_{i\sigma;i+n,\sigma'}(\omega) \\ G_{i-1,\sigma;i+n-1,\sigma'}(\omega) \\ G_{i-2,\sigma;i+n-2,\sigma'}(\omega) \\ \cdot \\ \cdot \\ \cdot \end{pmatrix}$$

be a vector of infinite length which contains all the propagators with the holes n sites apart. Of course, there are three entries replacing the $(0, n)$ entry, corresponding to sites a, b, d, and similarly for $(-n, 0)$. Further, we note that for $n \geq 1$, the ordering of the spins is preserved under hopping, since the left-most hole cannot pass by the right-most hole with one hop. Thus, we can write a recurrence relation for these vectors, for any $n \geq 1$, as:

$$\begin{pmatrix} \gamma_n & 0 \\ 0 & \gamma_n \end{pmatrix} \begin{pmatrix} V_n^{\uparrow\downarrow} \\ V_n^{\downarrow\uparrow} \end{pmatrix} = \begin{pmatrix} \alpha_n & 0 \\ 0 & \alpha_n \end{pmatrix} \begin{pmatrix} V_{n-1}^{\uparrow\downarrow} \\ V_{n-1}^{\downarrow\uparrow} \end{pmatrix} + \begin{pmatrix} \beta_n & 0 \\ 0 & \beta_n \end{pmatrix} \begin{pmatrix} V_{n+1}^{\uparrow\downarrow} \\ V_{n+1}^{\downarrow\uparrow} \end{pmatrix} \quad \text{(A1)}$$

where γ_n, α_n and β_n are very sparse matrices, whose elements can be read off from the equations of motion as in the periodic case. Further, as before, the tridiagonal form of the recurrence relation admits a continued fraction solution for these vectors. The rest of the procedure is the same as for the periodic case.

Truncation schemes of continued fractions:

(i) For this method to work we need to truncate the continued fraction at a large inter-hole separation M,

both for the periodic and impurity cases. In the periodic system, we start out by creating two holes on a TM site. The two holes can now delocalize in the system. However, the broadening η introduces a finite lifetime ($\sim 1/\eta$) so that $< k, 0, dd|G_P(\omega)|k, n, \alpha\beta > \longrightarrow 0$ as $n \longrightarrow \infty$. Thus for a large enough $n = M$, we can truncate the continued fraction for the V-vectors by setting V_{M_c+1} to zero.

For the impurity problem, this is justified because $G_{i\sigma;i+n,\sigma'}(\omega)$ is the Fourier transform of the amplitude of probability that the two holes move from the impurity (TM) site to the sites $i, i+n$ within a time τ. The larger n is, the less likely this process becomes, hence the smaller these propagators must be. This is certainly true for the energy ranges spanned by eigenstates that favor having the holes on the impurity (TM) site, since then they are unlikely to wander very far away from it. However, this is also true even if the holes preferred the O bath. This is because the broadening η is equivalent to introducing a finite lifetime $\sim 1/\eta$ for the holes, so they cannot move arbitrarily far in a finite time τ. Of course, in this latter case the appropriate cutoff M increases as η decreases. In practice, for both cases, we increase M until the results become insensitive to further changes.

(ii) A further truncation is necessary for the impurity problem. This is because, with the ordering of the propagators used for the V_n vectors, we have the additional complication that all these vectors, and therefore all the sparse matrices $\alpha_n, \beta_n, \gamma_n$, are infinitely-dimensional. In order to calculate the continued fractions, we need to truncate the size of these vectors, as well. The reasons discussed above justify doing this if either $|i| \gg 1$ and/or $|i+n| \gg 1$. We use the following truncation procedure: for a fixed separation n between the holes, the maximum distance either of the two holes is allowed to travel away from the TM is $R_c + n$, *i.e.*, we truncate $V_n^{\sigma,\sigma'}$ at $G_{R_c,\sigma;R_c+n,\sigma'}(\omega)$ at the top and $G_{-R_c-n+1;\sigma;-R_c+1,\sigma'}(\omega)$ at the bottom. Again, R_c is increased until results become independent of its value. As a final comment, we note that there are other ways of grouping the propagators into vectors so that the equations of motion still lead to a simple recursive relation. Different schemes have various computational advantages and disadvantages, but they all convergence to the correct answer if the cutoffs are sufficiently large. This converged result is equvalent to the exact solution computed by the Cini-Sawatzky theory for the Anderson impurity problem.

Appendix B: Choice of parameters

For simplicity, we discuss the impurity approximation first, and the full periodic system second.

For the impurity approximation, if we ignore the TM-bath hybridization, $V \to 0$, then if both holes are at the TM site the energy of the state is $E_\Omega^I - 2\Delta - U$; if one hole is at the TM site and one is in the O bath, the minimum energy of such states is $E_\Omega^I - \Delta - U - 2t - U_0$. Finally, if both holes are in the O bath, the minimum energy of such states is $E_\Omega^I - 4t - 2U_O$. As a result, the state with both holes at the TM atom is favorable energetically if $\Delta > 2t + U_0$ and $2\Delta + U > 4t + 2U_0$. The second condition is automatically satisfied if the first one holds, since the TM on-site interaction is repulsive, $U > 0$.

The condition $\Delta > 2t + U_0$ implies that AES should be more useful for Mott insulators than for charge transfer materials.[28] To see this, consider one-electron removal states from the GS. If the hole is removed from the TM site, the energy of the state is $E_\Omega^I - \Delta - U$, while if it is removed from an O site, the minimum energy is $E_\Omega^I - 2t - U_0$. The latter is energetically more expensive than the former if $\Delta > 2t + U_O$. This makes sense, because if the material was a charge transfer insulator the additional holes would prefer to stay in the O bath and AES would be less sensitive to the TM atom specific properties.

The analysis for the periodic system is very similar for $V \to 0$, because the energy differences between states having (i) both holes at the same TM site, (ii) one hole at a TM site and one in the O bath, and (iii) both holes in the O bath, are precisely the same as for the impurity case. Because of this and also in order to be able to meaningfully compare with impurity approximation results, we use the same parameters in both cases.

Note that in the periodic system we can also have (iv) the two holes at different TM sites. For $V = 0$, these states has energy $E_\Omega^P - 2\Delta - 2U$ and are always energetically favored compared to having both holes at the same TM site. Of course, these are the states projected out in our variational calculation.

[1] B. Feuerbacher, B. Fitton, and R. Willis, *Photoemission and the electronic properties of surfaces* (Wiley, 1978).
[2] D. Chattarji, *The theory of Auger transitions* (Academic Press, 1976).
[3] E. Antonides, E. C. Janse, and G. A. Sawatzky, Phys. Rev. B **15**, 1669 (1977).
[4] D. E. Ramaker, Critical Reviews in Solid State and Materials Sciences **17**, 211 (1991).
[5] L. C. Davis, Journal of Applied Physics **59**, R25 (1986).
[6] J. Ghijsen, L. H. Tjeng, J. van Elp, H. Eskes, J. Westerink, G. A. Sawatzky, and M. T. Czyzyk Phys. Rev. B **38**, 11322 (1988).
[7] M. Cini, Solid State Communications **24**, 681 (1977).
[8] M. Cini, Solid State Communications **20**, 605 (1976).
[9] G. A. Sawatzky, Phys. Rev. Lett. **39**, 504 (1977).
[10] M. Potthoff, in Band-Ferromagnetism, Lecture Notes in Physics, Vol. 580 (Springer Berlin Heidelberg, 2001) pp. 356-370.
[11] M. Cini, Phys. Rev. B **17**, 2486 (1978).
[12] M. Cini and A. D'Andrea, Phys. Rev. B **29**, 6540 (1984).

[13] M. Cini, Phys. Rev. B **32**, 1945 (1985).
[14] C. Verdozzi and M. Cini, Phys. Rev. B **51**, 7412 (1995).
[15] M. Cini, A. Pernaselci, and E. Paparazzo, Journal of Electron Spectroscopy and Related Phenomena **72**, 77 (1995).
[16] A. Pernaselci and M. Cini, Journal of Electron Spectroscopy and Related Phenomena **82**, 79 (1996).
[17] P.-O. Löwdin, Journal of Chemical Physics **18**, 365 (1950).
[18] O. Gunnarsson, K. Schönhammer, J. C. Fuggle and R. Lässer, Phys. Rev. B **23**, 4350 (1981).
[19] C. Verdozzi, M. Cini, and A. Marini, Journal of Electron Spectroscopy and Related Phenomena **41**, 117118 (2001).
[20] A. Marini and M. Cini, Phys. Rev. B **60**, 11391 (1999).
[21] P. W. Anderson, Phys. Rev. **124**, 41 (1961).
[22] O. Gunnarsson and K. Schöhammer, Phys. Rev. B **28**, 4315 (1983).
[23] J. Zaanen, C. Westra and G. A. Sawatzky, Phys. Rev. B **33**, 8060 (1986).
[24] H. Eskes and G. A. Sawatzky, Phys. Rev. B **44**, 9656 (1991).
[25] M. Berciu, Phys. Rev. Lett. **107**, 246403 (2011).
[26] M. Möller, A. Mukherjee, C. P. J. Adolphs, D. J. J. Marchand, and M. Berciu, Journal of Physics A: Mathematical and Theoretical **45**, 115206 (2012).
[27] M. Berciu and A. M. Cook, Europhys. Lett. **92**, 40003 (2010).
[28] J. Zaanen, G. A. Sawatzky and J. W. Allen, Phys. Rev. Lett. **55**, 418 (1985).